PCCP

PAPER

View Article Online
View Journal | View Issue

Cite this: *Phys. Chem. Chem. Phys.*, 2014, **16**, 10629

Complex refractive indices in the near-ultraviolet spectral region of biogenic secondary organic aerosol aged with ammonia

J. M. Flores,[a] R. A. Washenfelder,[bc] G. Adler,[a] H. J. Lee,[d] L. Segev,[a] J. Laskin,[e] A. Laskin,[f] S. A. Nizkorodov,[d] S. S. Brown[c] and Y. Rudich*[a]

Received 9th March 2014,
Accepted 10th April 2014

DOI: 10.1039/c4cp01009d

www.rsc.org/pccp

Atmospheric absorption by brown carbon aerosol may play an important role in global radiative forcing. Brown carbon arises from both primary and secondary sources, but the mechanisms and reactions of the latter are highly uncertain. One proposed mechanism is the reaction of ammonia or amino acids with carbonyl products in secondary organic aerosol (SOA). We generated SOA *in situ* by reacting biogenic alkenes (α-pinene, limonene, and α-humulene) with excess ozone, humidifying the resulting aerosol, and reacting the humidified aerosol with gaseous ammonia. We determined the complex refractive indices (RI) in the 360–420 nm range for these aerosols using broadband cavity enhanced spectroscopy (BBCES). The average real part (n) of the measured spectral range of the NH_3-aged α-pinene SOA increased from n = 1.50 (±0.01) for the unreacted SOA to n = 1.57 (±0.01) after 1.5 h of exposure to 1.9 ppm NH_3, whereas the imaginary component (k) remained below $k < 0.001\left(^{+0.002}_{-0.001}\right)$. For the limonene and α-humulene SOA the real part did not change significantly, and we observed a small change in the imaginary component of the RI. The imaginary component increased from k = 0.000 to an average k = 0.029 (±0.021) for α-humulene SOA, and from $k < 0.001\left(^{+0.002}_{-0.001}\right)$ to an average k = 0.032 (±0.019) for limonene SOA after 1.5 h of exposure to 1.3 and 1.9 ppm of NH_3, respectively. Collected filter samples of the aged and unreacted α-pinene SOA and limonene SOA were analyzed off-line by nanospray desorption electrospray ionization high resolution mass spectrometry (nano-DESI/HR-MS), and *in situ* using a Time-of-Flight Aerosol Mass Spectrometer (ToF-AMS), confirming that the SOA reacted and that various nitrogen-containing reaction products formed. If we assume that NH_3 aging reactions scale linearly with time and concentration, which will not necessarily be the case in the atmosphere, then a 1.5 h reaction with 1 ppm NH_3 in the laboratory is equivalent to 24 h reaction with 63 ppbv NH_3, indicating that the observed aerosol absorption will be limited to atmospheric regions with high NH_3 concentrations.

1. Introduction

Atmospheric aerosols play an important role in the Earth's radiative budget by absorbing and scattering solar radiation and by influencing cloud properties.[1] Light-absorbing aerosols (including black carbon, mineral dust, and brown carbon) are recognized to have a potentially important role in climate radiative forcing.[2–7] Atmospheric brown carbon (BrC) refers to light-absorbing organic particulate matter, which can be generated both from primary sources (*e.g.*, combustion, biomass burning, soil humics, bioaerosols) and from secondary organic reactions (*e.g.*, particle or aqueous-phase reactions).[8] The interest and climatic importance of BrC aerosol are due to the strong dependence of its absorption on its composition, the complexity of its production mechanisms, and the poor constraints on its contribution to radiative forcing.[6,8–14] Only recently, studies have shown that brown carbon aerosol may account for 10 to 50% of the total light absorption in the atmosphere, snow, and sea ice.[3–5,11,15–18]

Primary emissions of BrC have been observed in wildfire events,[6] residential coal combustion,[14] and release of biological aerosols (for example, fungi, plant debris, and humic matter).[19] In addition to primary emissions, BrC compounds may occur in

[a] *Department of Earth and Planetary Sciences, Weizmann Institute of Science, Rehovot 76100, Israel. E-mail: yinon.rudich@weizmann.ac.il*
[b] *Cooperative Institute for Research in Environmental Sciences, University of Colorado, 216 UCB, Boulder, CO 80309, USA*
[c] *Chemical Sciences Division, Earth System Research Laboratory, National Oceanic and Atmospheric Administration, 325 Broadway, Boulder, CO 80305, USA*
[d] *Department of Chemistry, University of California, Irvine, CA 92697, USA*
[e] *Physical Sciences Division, Pacific Northwest National Laboratory, Richland, WA 99352, USA*
[f] *Environmental Molecular Sciences Laboratory, Pacific Northwest National Laboratory, Richland, WA 99352, USA*

secondary organic aerosol (SOA) consisting of high molecular weight and multifunctional species, such as humic-like substances, organonitrates, and organosulfates. The principal precursors, mechanisms, and products in the formation of secondary BrC are poorly known, and different reactions and mechanisms have been proposed to explain the light absorption by secondary organic aerosol:

(1) Reaction of ammonia (NH_3) or amino acids with secondary organic aerosol that contains carbonyl products.[20–23] This category of reactions may further include aqueous reactions of glyoxal and methylglyoxal with ammonium sulfate,[24–28] aqueous reactions between glyoxal and amino acids,[24,26,29] and gas-to-particle uptake of glyoxal by deliquesced AS and amino acid-containing aerosol.[30–33] A proposed mechanism for the ammonia reaction with carbonyls starts with conversion of protonated carbonyls into primary imines and amines (R1a), which then react with additional carbonyls to produce more stable secondary imines (R1b) and heterocyclic (R1c) nitrogen containing compounds. The products of these reactions may continue to react with unreacted carbonyl groups yielding higher molecular weight molecules with an extended network of conjugated bonds.[21]

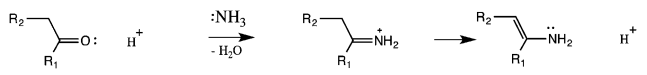

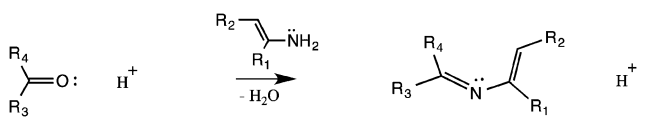

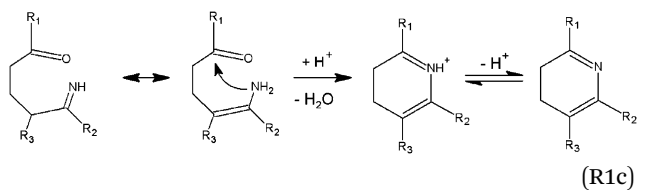

(2) Acid-catalyzed aldol condensation of volatile aldehydes,[34–41] which is only expected to be important under H_2SO_4 concentrations characteristic of stratospheric aerosols.

(3) Nitration of polycyclic aromatic hydrocarbons (PAH) leading to light absorbing nitro-PAH, and their derivatives such as nitrophenols.[42–45]

(4) Other proposed mechanisms such as reaction of OH radicals with aromatic hydroxyacids and phenols in cloud water,[46–49] heterogeneous reactions of gas-phase isoprene on acidic aerosol particles,[50] and aqueous photochemistry of pyruvic acid in the presence of common atmospheric electrolytes (*e.g.*, SO_4^{2-}, NH_4^+).[51,52]

The majority of the studies summarized above use bulk solution-phase reactions to simulate aerosol-aging mechanisms. It is critical to study this chemistry *in situ* by realistic aerosol size distributions, as bulk-phase reactions may be limited by the rate of transport of gaseous reactants and products in and out of the condensed phase. Furthermore, *in situ* measurements are necessary to evaluate the influence of aging mechanisms on aerosol optical properties as they may occur in the atmosphere. SOA optical extinction and refractive indices at selected wavelengths in the UV and visible spectral regions have been measured in the laboratory,[53–63] with a few measurements throughout the visible spectrum.[53,55,64] Recent advances in broadband cavity enhanced spectroscopy (BBCES) allow aerosol optical extinction, optical cross section, and the real (scattering) and imaginary (absorption) components of the refractive index to be determined as a function of wavelength.[65–67] Here, we use the instrument described in Washenfelder *et al.* (2013)[65] to measure optical properties in the near-UV spectral region of SOA formed by the reaction of biogenic alkenes with ozone, and by subsequent reaction with NH_3.

Based on the study by Updyke *et al.* (2012)[23] we select biogenic alkenes that form SOA that can undergo different degrees of "browning" (*i.e.*, a visible change in color or measured absorption spectrum) upon exposure to NH_3. In each case, we measure the aerosol optical extinction coefficient and cross section, and we use these quantities to retrieve the refractive index before and after SOA reactions with gas-phase NH_3. We compare our results to the imaginary part of the refractive index determined by ultraviolet/visible (UV/Vis) absorption of solution-phase products, and assess the climatic importance using the "simple forcing efficiency" (SFE) defined by Bond and Bergstrom (2006).[68]

2. Experimental

2.1. Generation of NH_3-aged biogenic SOA

The flow system for aerosol generation and aging is shown schematically in Fig. 1A and described in detail below. SOA was generated by ozonolysis of three different biogenic alkenes: α-pinene, limonene and α-humulene. The liquid volatile organic compound (VOC) was injected using a syringe pump at 0.7–4.1 μL h^{-1} into a N_2 carrier gas flow of 0.4 volumetric liters per minute (vlpm). O_3 was generated by passing 0.1 vlpm of moisture-free O_2 through a commercial Double-Bore UV lamp (Jelight Company Inc., Irvine, CA, USA). The two flows were combined in a 10 L bulb, to give an initial VOC concentration of ~10 parts per million by volume (ppmv) for the upper limit infusion rate from the syringe pump. The O_3 mixing ratio was measured to be 90 (±10) ppm using a commercial O_3 monitor (Model 1180, Dasibi Environmental Corp., Glendale, CA, USA). The ozone + VOC reaction took place under dark conditions. After the reaction bulb, an ozone denuder (Carulite 200; Carus Corp., Peru, IL, USA) removed the residual O_3 from the sample flow. The SOA flow was then humidified to 85% relative humidity (RH) using a Nafion humidifier (PermaPure LLC, Toms River, NJ, USA) with a temperature-controlled bath. BrC formation upon exposure to NH_3 has only been observed under humid conditions (RH ~85%).[21] The humidified SOA was introduced to a 30 L flow tube where it was combined with gaseous NH_3 and allowed to react for 1.5 h. The SOA was then dried to <10% RH using a diffusion dryer and the residual NH_3 was removed using silicon phosphate pellets (AS-200-08-E, Perma Pure LLC., Toms River, NJ, USA), before being size-selected using a differential mobility analyzer (DMA; Model 3081, TSI Inc., Shoreview, MN, USA). The size-selected aerosol

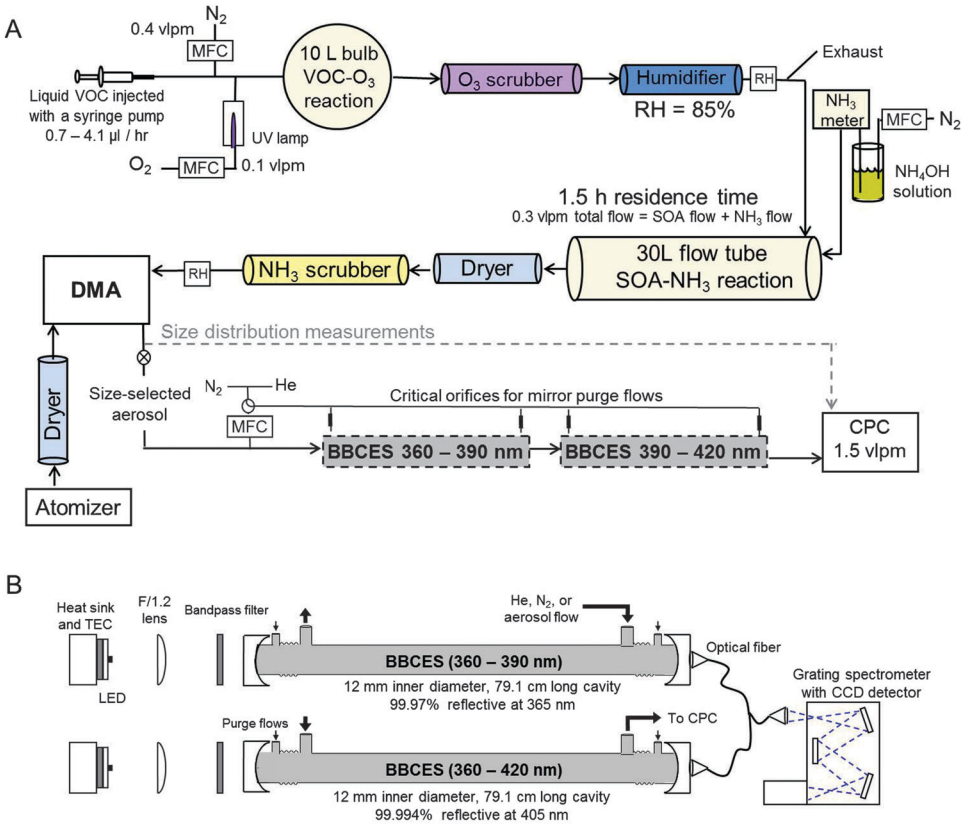

Fig. 1 (A) Schematic diagram of the experimental system for generating SOA from reaction of biogenic alkenes with ozone, followed by aging with NH_3 gas. (B) The broadband cavity enhanced spectrometer, with channels for 360–390 and 390–420 nm. Relative humidity measurements are marked as "RH". Acronyms: MFC – mass flow controller, DMA – differential mobility analyzer, BBCES – broadband cavity enhance spectrometer, CPC – condensation particle counter, TEC – thermoelectric cooler, LED – light emitting diode.

was introduced to the two BBCES cells in series and finally counted using a condensation particle counter (CPC; Model 3775, TSI Inc., Shoreview, MN, USA). For measurements without NH_3, the SOA was passed through the same setup without the addition of NH_3 in the 30 L bulb. The reaction time in the bulb was sufficient to generate a stable aerosol population of VOC oxidation products, with the mode diameter typically near 200 nm and total mass concentrations of 1100 ($\pm$100) µg m^{-3}.

NH_3 gas was generated by bubbling 0.005 to 0.04 vlpm N_2 through a 10 mM NH_4OH solution. The NH_3 concentration was measured using an NH_3 detector (Model TX-2460DP-D, Bionics Instrument Co. Ltd., Tokyo, Japan) before it entered the 30 L flow tube to react with the humidified SOA. To control the concentration of ammonia that was introduced into the flow tube, and to determine the residence time, a constant total flow of 0.3 vlpm was maintained in the flow tube throughout the experiments. By changing the N_2 flow through the NH_4OH solution, different NH_3 concentrations were introduced while maintaining the same total flow in the system. The relative humidity of the NH_3 flow varied between 70% at 0.005 vlpm and 86% at 0.04 vlpm, resulting in a relative humidity for the total aerosol flow of 85% $\pm$ 2%.

2.2. Broadband cavity enhanced extinction spectroscopy (BBCES)

The BBCES technique employs a broadband light source, a high-finesse optical cavity, a grating spectrometer and a multichannel detector to simultaneously determine optical extinction across a broad wavelength region.[69] Initial measurements demonstrated its potential to measure the optical extinction of ambient aerosol,[70–73] and recent studies have demonstrated how the technique may be combined with aerosol size-selection to determine aerosol extinction cross sections and refractive indices as a function of wavelength.[63,65,67]

The optical instrument used in this study consists of two channels to measure aerosol optical extinction from 360 to 390 nm and 390 to 420 nm, respectively. It is similar to the instrument described in detail in Washenfelder *et al.* (2013)[65] and briefly summarized here. Fig. 1B shows a schematic of the BBCES system used in this study.

Light emitting diodes (LEDs) centered at 370.2 and 407.1 nm with measured optical power outputs of 0.210 W and 0.450 W (NCSU033A, Nichia Corp., Tokyo, Japan; LZ1-00UA05, LEDEngin Inc., San Jose, CA, USA) are temperature-controlled and powered by a constant-current power supply to achieve a stable optical power output. The output from each LED is collimated using a single F/1.2 fused silica lens into an optical cavity formed by two 2.5 cm, 1 m radius of curvature mirrors (Advanced Thin Films, Boulder, CO, USA). The measured mirror reflectivity for the two cavities was typically 0.9995 and 0.99994 at 370 and 407 nm, respectively. The light entering the cavity is optically filtered using bandpass filters (FGUV5 and FB400-40, Thorlabs, Newton, NJ, USA).

After exiting each cavity, the light is directly collected using a 0.1 cm F/2 fiber collimator (74-UV, Ocean Optics, Dunedin, FL, USA) into one lead of a two-way 100 μm core HOH-UV-VIS fiber (SR-OPT-8015, Andor Techonology, Belfast, UK) which is linearly aligned along the input slit of the grating spectrometer.

Spectra were acquired using a 163 mm focal length Czerny-Turner spectrometer (Shamrock SR-163, Andor Technology, Belfast, UK) equipped with a charge coupled device (CCD) detector (DU920P-BU, Andor Technology, Belfast, UK) maintained at −50 °C. The installed 300 groove mm^{-1} (500 nm blaze) grating allows spectral measurements over the region 101–621 nm, although only a portion of that spectral region was used in these experiments. The spectrometer is temperature-controlled at 32.0 (±0.1) °C. Dark spectra were acquired using the input shutter (SR1-SHT-9003, Andor Technology, Belfast, UK) closed prior to each set of spectra. The wavelength calibration was determined using a Hg/Ar pen-ray lamp. The 100 μm fiber from each measurement channel illuminated separate vertical regions of the CCD, which were digitized to produce two spectra.

The general expression that relates the extinction coefficient by aerosols, $\alpha(\lambda)$ measured in cm^{-1}, in an N_2-filled cavity, to the change in intensity of the transmitted light is given by:

$$\alpha_{\text{ext}}(\lambda) = R_L\left(\frac{(1-R(\lambda))}{d} + \alpha_{\text{Rayleigh N}_2(\lambda)}\right)\left(\frac{I_{N_2}(\lambda) - I(\lambda)}{I(\lambda)}\right) \quad (1)$$

where R_L is the ratio of the total length (d) to the filled length of the cavity, $R(\lambda)$ is the mirror reflectivity, $\alpha_{\text{Rayleigh N}_2(\lambda)}$ is the extinction coefficient due to Rayleigh scattering by N_2, $I_{N_2}(\lambda)$ is the spectrum (*i.e.*, the wavelength-dependent intensity transmitted through the cavity and imaged to the CCD) of N_2, and $I(\lambda)$ is the spectrum with aerosol and N_2 present.[65] Using the particle number concentration (N) measured by the CPC, the optical extinction cross section, $\sigma(\lambda)$ measured in cm^2, at each wavelength can be calculated:

$$\sigma_{\text{ext}}(\lambda) = \frac{\alpha_{\text{ext}}(\lambda)}{N} \quad (2)$$

For spherical particles, the measurement of several diameters allows the retrieval of the complex refractive index at each wavelength by minimizing the expression

$$\chi^2(\lambda) = \sum_{i=1}^{N_{D_p}} \left(\frac{\sigma_{\text{ext,measured}}(\lambda) - \sigma_{\text{ext,calculated}}(\lambda)}{\sigma_{\text{ext,measured}}(\lambda)}\right)_i^2 \quad (3)$$

where N_{D_p} is the number of diameters measured and $\sigma_{\text{ext,calculated}}$ is the theoretical optical cross section calculated using Mie theory by varying the real (n) and imaginary (k) components of the complex refractive index (RI).[65] We account for the contribution of multiply-charged particles by calculating the size distribution exiting the DMA for each diameter using DMA transfer theory[74] and steady-state charge distribution approximation.[75]

2.3. Operational details for *in situ* generation and sampling

The aerosol generation, including VOC, O_3, and NH_3 flows, temperatures, and other components, were allowed to stabilize for at least 1 h prior to each set of measurements. A scanning mobility particle sizer (SMPS) was used to verify that the aerosol size distribution was stable prior to the measurements. After the aerosol size distribution stabilized, an SMPS scan was taken for multiple-charge correction while the BBCES reflectivity term in eqn (1) was determined by recording spectra with the cavity filled by He and N_2 sequentially.[70] Next, a zero-particle measurement was performed followed by measurements with a series of size selected particles, typically in the range of D_p = 200–450 nm in 50 nm increments. After the size-selection measurements, another zero-particle, reflectivity and size distribution measurement was performed. Measurements with polystyrene latex spheres (PSL) of known sizes were performed to evaluate the performance of the experimental setup either before or after each experiment.

2.4. UV/visible absorption spectroscopy

In addition to the *in situ* generation of aerosol and measurement of optical extinction described above, we used a UV/Vis spectrometer (Cary 100 UV-Vis, Agilent Technologies Inc., Santa Clara, CA, USA) to measure absorption by aerosols dissolved in aqueous solution. Besides the refractive index, another standard metric of aerosol absorption in the UV/Vis region is the mass absorption coefficient (MAC), given in units of $m^2\ g^{-1}$:

$$\text{MAC}(\lambda) = \frac{A(\lambda)\ln(10)}{Cb} \quad (4)$$

where $A(\lambda)$ is the base-10 absorbance measurement (unitless), C is the concentration of the liquid solution ($g\ m^{-3}$), and b is the sample path length (m).[76] The relationship between k and the MAC is

$$\text{MAC} = \frac{4\pi k}{\rho_{\text{material}}\lambda} \quad (5)$$

where ρ_{material} is the density of the organic material.[76] For our measurements, we assume a density of 1.4 $g\ cm^{-3}$, which is a recommended value for biogenic SOA.[77] UV/Vis absorption spectroscopy cannot be used to determine the real part of the refractive index. For an assumed density of 1.4 $g\ cm^{-3}$ and a wavelength of 400 nm, a k value of 0.01 corresponds to MAC = 0.22 $m^2\ g^{-1}$, while a k value of 0.05 corresponds to MAC = 1.12 $m^2\ g^{-1}$.

2.5. Analysis of aerosol composition

We used two methods to determine the chemical composition of the *in situ* aerosol described above: Time-of-Flight Aerosol Mass Spectrometry (ToF-AMS) and nanospray Desorption Electrospray Ionization High Resolution Mass Spectrometry (nano-DESI/HR-MS).

ToF-AMS. For α-pinene and limonene, we generated SOA and aged the aerosol with 1 ppmv of NH_3, as described in Section 2.1. We analyzed *in situ* both NH_3-aged and unreacted α-pinene and limonene SOA using a ToF-AMS (Aerodyne Research, Inc., Billerica, MA, USA) connected directly to the experimental setup. A detailed description of the ToF-AMS can be found in DeCarlo *et al.* (2006).[78] The Tof-AMS operated in the more sensitive V-mode ion path[78] with the results presented here obtained using the mass spectrum (MS) mode (in which the ion signals are integrated over all particle sizes). Data analysis of the MS was done using Squirrel v.1.51H.

Nano-DESI/HR-MS. We collected filter (Whatman 2 μm PTFE 46.2 mm 7592-104, Whatman Inc., Florham Park, NJ, USA) samples of limonene SOA and α-pinene SOA, before and after aging by NH_3. The filters were analyzed using a high-resolution LTQ-Orbitrap MS (Thermo Fisher, Bremen, Germany) equipped with a nano-DESI source,[79,80] followed by assignment of molecular formulae to the observed peaks using the procedure described in Roach *et al.* (2011).[81] The instrument was operated in the positive-ion mode with a resolving power of 100 000 at m/z 400, and calibrated using a standard calibration mixture (Calibration mix MSCAL 5, Sigma-Aldrich Co. LLC, St. Louis, MO, USA). A voltage of 3–4 kV was applied between the capillary end and the mass spectrometer inlet to obtain a stable spray of charged droplets. The solvent (acetonitrile/water mixed at 70/30 volumetric ratio) was supplied at a 2–3 μL min^{-1} flow rate to maintain a stable nano-DESI probe on the sample surface.

2.6. Radiative impact

To estimate the direct radiative forcing in watts per gram, Bond and Bergstrom (2006)[68] modified the forcing equation of Chylek and Wong (1995),[82] to give a "simple forcing efficiency" (SFE, W g^{-1}). We used the wavelength-dependent version[76] to provide an estimate of the radiative impact of the aged SOA:

$$\frac{\mathrm{dSFE}}{\mathrm{d}\lambda} = -\frac{1}{4}\frac{\mathrm{d}S(\lambda)}{\mathrm{d}\lambda}\tau_{\mathrm{atm}}{}^2(\lambda)(1-F_{\mathrm{c}})\left[2(1-a_{\mathrm{s}})^2\beta(\lambda)\cdot\mathrm{MSC}(\lambda) - 4a_{\mathrm{s}}\cdot\mathrm{MAC}(\lambda)\right] \quad (6)$$

where $\mathrm{d}S(\lambda)/\mathrm{d}\lambda$ is the solar irradiance, τ_{atm} is the atmospheric transmission, F_{c} is the cloud fraction (0.6), a_{s} is the surface albedo (average of 0.19), β is the backscatter fraction, and MSC is the mass scattering.

3. Results and discussion

3.1. Refractive indices of NH_3-aged biogenic SOA measured *in situ* by BBCES

The reaction of each biogenic VOC with O_3 for 20 min produced stable SOA size distributions. During the 1.5 h reaction of these aerosols with NH_3, this size distribution shifted to larger diameters and the number of particles decreased, which can be attributed to coagulation and loss of the particles to the walls of the flow tube.

The retrieved complex refractive indices are shown in Fig. 2 as a function of wavelength between 360 and 420 nm for the three different SOA. The biogenic alkenes are arranged in the order of increasing absorption for their NH_3-aged SOA, based on the study of Updyke *et al.* (2012).[23] Refractive indices of α-pinene SOA and its aging at three NH_3 concentrations (0.3 ppm, 1.0 ppm, and 1.9 ppm) are shown in Fig. 2A. There is no detectable absorption for the α-pinene SOA, with an average imaginary component over the 360–420 nm range of $k < 0.001\left(^{+0.002}_{-0.001}\right)$ even after 1.5 h of aging with 1.9 ppm of NH_3. However, there is an increase in the real part of the RI, from an average $n = 1.50$ (±0.01) to $n = 1.53$ (±0.02) with the addition of 0.3 ppm NH_3, and a greater increase up to an average $n = 1.57$ (±0.01) with 1.9 ppmv NH_3. The increase might be attributed to an increase in the density of the aerosol.[63,83] The α-humulene SOA in Fig. 2B shows no increase in the real part of the RI, but the imaginary component increases to an average value of $k = 0.029$ (±0.021) at NH_3 concentration greater than 1.0 ppm. The limonene SOA in Fig. 2C similarly shows that the real part of the RI remains constant at all NH_3 concentrations, and there is a small increase in the imaginary component of the RI ($k = 0.032$ (±0.019)) when the aerosol is aged with 1.9 ppm NH_3. The refractive indices of all of these SOA show a wavelength-dependent real part between 1.47 and 1.59 and an imaginary part less than 0.07. The error bars in Fig. 2 were calculated by scaling the measured extinction cross sections by the total measurement uncertainty (<4%).[65]

The BBCES measurements and retrieved refractive indices indicated minor or no detectable absorption by the *in situ* NH_3-aged aerosol with $[NH_3] < 1.0$ ppm in the 360–420 nm range. To understand this result, we undertook a series of additional experiments described in Sections 3.2–3.4. First, we used the BBCES to measure refractive indices of atomized Suwannee River Fulvic Acid (SRFA) and atomized NH_3-aged limonene SOA samples generated in a different laboratory (Section 3.2). Second, we used UV/Vis absorption spectroscopy to determine the absorption of SRFA and NH_3-aged aerosol in aqueous solution (Section 3.3). Finally, we analyzed the chemical composition of the NH_3-aged aerosol generated in our laboratory using nano-DESI/HR-MS and ToF-AMS to verify that the expected chemical products had been formed.

3.2. Refractive indices of atomized samples measured by BBCES

We measured extinction cross sections of aerosolized SRFA material (1S101F International Humic Substances Society, Saint Paul, MN, USA), which is often used as a proxy for brown carbon, to verify that there were no errors with the instrumental method or the refractive index retrieval, and to confirm the small absorption values determined for the NH_3-aged SOA. The aerosol was generated by atomizing an aqueous SRFA solution followed by drying and size selection. The retrieved RI values are shown in Fig. 3A, with a clearly-detectable absorption having an average retrieved value of $k = 0.046$ (±0.010) in the 360–420 nm spectral region, consistent with previous work.[65]

We measured an atomized aerosol from a filter sample of NH_3-aged limonene SOA that was generated at the University of California, Irvine by bubbling O_3 gas through an acetonitrile solution containing limonene at room temperature until all double bonds were consumed. Then an aqueous solution of ammonium sulfate was added, and the mixture was evaporated to produce an orange-colored residue. The organic fraction was extracted with acetonitrile and dried for storage and shipment. Oxidation of limonene in a non-participating solvent such as acetonitrile is expected to produce a similar set of products as in the gas-phase oxidation of limonene. The optical properties of the resulting SOA material were slightly different to that of limonene SOA aged by the method described in Updyke *et al.* (2012).[23] The UC

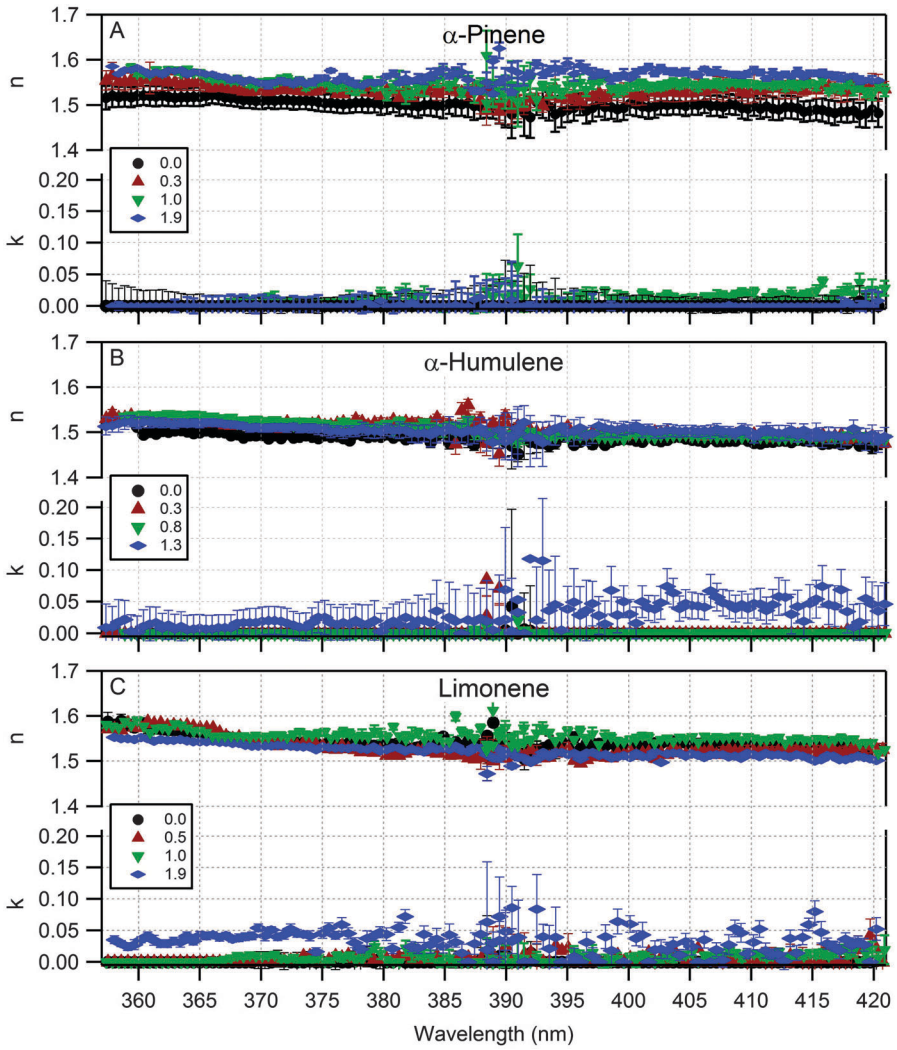

Fig. 2 Retrieved complex refractive indices as a function of wavelength for the unreacted biogenic SOA (black circles) and NH_3-aged biogenic SOA (red triangles, green inverted triangles, and blue diamonds) for (A) α-pinene, (B) α-humulene, and (C) limonene. The legend indicates the NH_3 concentration (ppmv) added. For all experiments the aerosols were humidified to 85% RH before being mixed with NH_3.

Irvine filter sample was dissolved in acetonitrile and water, and atomized for measurement with the BBCES using the size-selection procedure and RI retrieval. Fig. 3A shows that for the aerosol there was no detectable absorption in the 360–420 nm range, with a retrieved k value equal to zero $\left(^{+0.022}_{-0.000}\right)$ within experimental uncertainties, consistent with the results for the *in situ* NH_3-aged limonene SOA with lower NH_3 concentrations generated in our laboratory.

3.3. Refractive indices of NH_3-aged biogenic SOA measured by UV/Vis spectroscopy

The atomization of the filter samples described in Section 3.2 showed that the NH_3-aged biogenic SOA was much less absorbing than SRFA at 360–420 nm. We used UV/Vis absorption spectroscopy to measure and compare the absorption of three aqueous samples: SRFA, NH_3-aged limonene SOA generated at UC Irvine, and NH_3-aged limonene SOA generated using the flow tube system shown in Fig. 1 with ~1 ppmv NH_3 and collected on a filter for approximately 6 h.

For the UV/Vis spectra, the SRFA was dissolved in nanopure water, UC Irvine NH_3-aged limonene SOA was dissolved in acetronitrile (CH_3CN), and the Weizmann Institute NH_3-aged limonene SOA in nano-pure water and methanol. We prepared three mass concentrations for each of the three materials. Fig. 3B shows that both filter samples of NH_3-aged limonene SOA are an order of magnitude less absorbing than SRFA. The NH_3-aged limonene SOA from Updyke *et al.* (2012)[23] (see their Fig. 4) is also overlaid for comparison. It is also an order of magnitude less absorbing than SRFA in the 360–420 nm range and 31% less absorbing at the peak seen around 500 nm. This is consistent with our BBCES *in situ* measurements of the atomized filter samples which showed that SRFA was more strongly absorbing than NH_3-aged limonene SOA (Section 3.2) and with the refractive index retrievals for the *in situ* NH_3-aged SOA. To directly compare the results from the UV-Vis and the

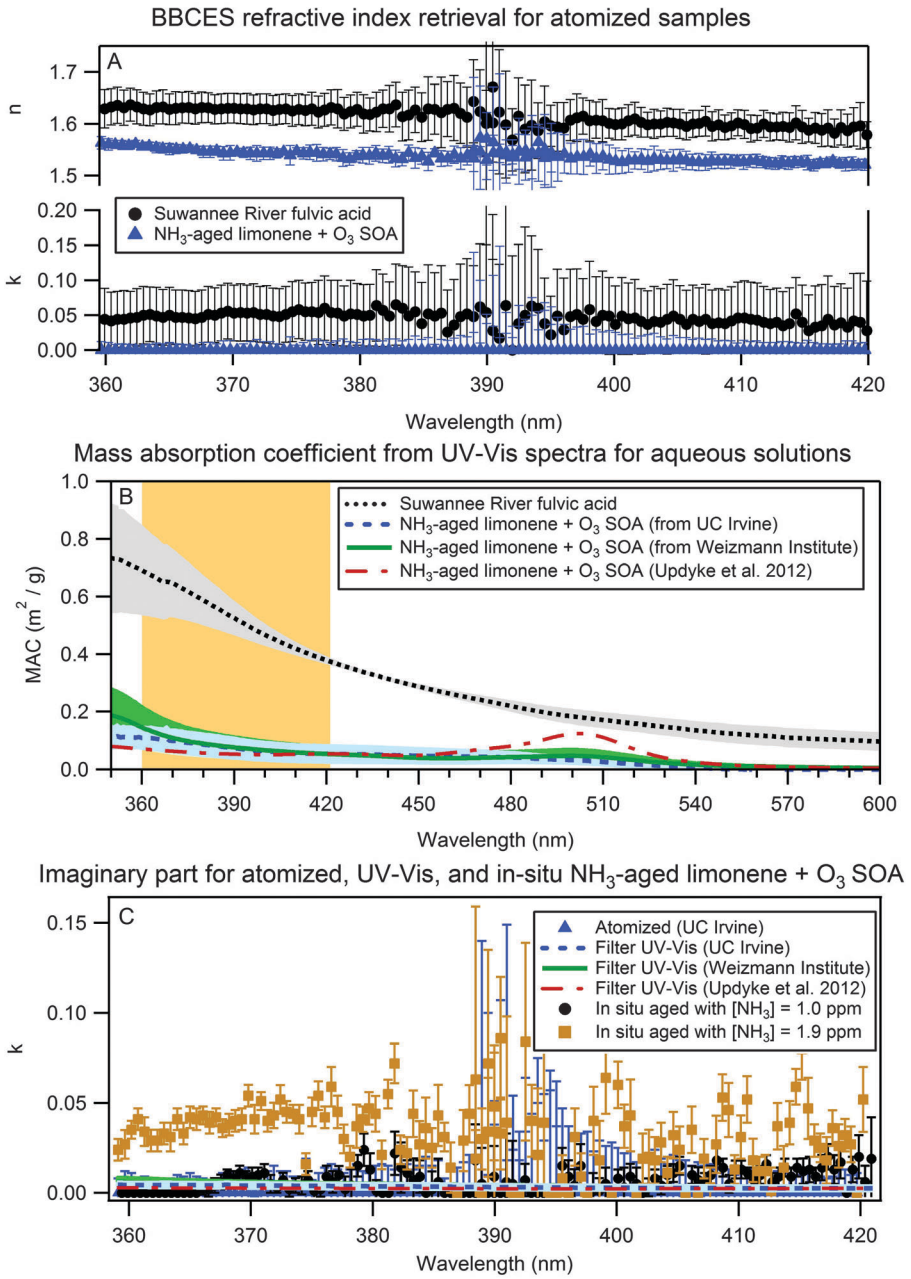

Fig. 3 (A) Retrieved complex refractive indices as a function of wavelength from BBCES size selection measurements for Suwannee River fulvic acid aerosols (black circles) and for NH_3-aged limonene SOA on a filter, extracted into liquid and atomized (blue triangles). (B) Mass absorption coefficient (MAC) for Suwannee River fulvic acid (dotted black line), NH_3-aged limonene SOA on a filter (blue dashed line), limonene SOA aged *in situ* and consequently extracted from the filter sample (green line) and from Updyke *et al.*[23] (red dash-dotted line). The shaded area in each trace shows the standard deviation of three different solution concentration measurements using a UV-Vis spectrometer. The orange area indicates the measurement range of the BBCES. (C) Calculated imaginary part from the MAC measurements in panel B (assuming a particle density of 1.4 g cm^{-3}) as a function of wavelength for the NH_3-aged limonene SOA (same color legend as in panel B), compared to the retrieved *k* values of limonene SOA aged with [NH_3] = 1.0 ppm (black circles) and [NH_3] = 1.9 ppm (orange squares) and the atomized sample (blue triangles; same as in panel A) from BBCES size selection measurements.

atomized and *in situ* BBCES measurements of the NH_3-aged limonene SOA, Fig. 3C shows calculated *k* values from the MAC values shown in Fig. 3B (using eqn (5) and assuming a $\rho_{material}$ = 1.4 g cm^{-3}), and the retrieved imaginary parts from the atomized and *in situ* BBCES measurements. Fig. 3C further shows the consistency of the UV-Vis and our BBCES *in situ* measurements. Based on the *in situ* BBCES measurements and the UV/Vis spectroscopy, we conclude that the NH_3-aged biogenic samples, although light orange in color, are substantially less absorbing than SRFA when normalized per unit mass of the material, in the measured wavelength region and under our experimental conditions.

Filter samples of α-pinene and limonene SOA before and after NH_3-aging were collected as described above and also

examined visually. Filter samples of α-pinene SOA appeared white, with or without NH_3-aging. Filter samples of unreacted limonene SOA also appeared white, while limonene SOA that was exposed *in situ* to ~1 ppmv NH_3 for 1.5 h was light orange in color, confirming that the NH_3 exposure caused visible changes in the optical properties of the aerosol. The light orange color does not arise from absorption in the 360–420 nm range, and is likely the result of absorption near 500 nm.

3.4. Composition of NH_3-aged biogenic SOA measured by nano-DESI/HR-MS and ToF-AMS

Nano-DESI-HRMS analysis. The chemical aging of limonene SOA and α-pinene SOA by NH_3 has been previously reported.[21–23,84] Fig. 4 shows a histogram of the number of N and O atoms from the identified peaks in the nano-DESI/HR-MS spectra of the α-pinene SOA and limonene SOA with and without aging by NH_3. In Fig. 4A and B, the unreacted α-pinene SOA and limonene SOA spectra show that >96% of the fragments contain zero N atoms and <4% of the fragments contain one N atom. The species with one N atom likely originate from trace amounts of NH_3 emitted by the walls of the flow tube or are introduced during SOA sample handling from ammonia in ambient air. The unreacted SOA is mainly composed of organic molecules containing C, H, and O atoms. In contrast, the NH_3-aged samples show a significant increase in the fraction of organic constituents with one or two N atoms (1N and 2N, respectively). For NH_3-aged α-pinene SOA, the sample contained 26% and 2% of 1N and 2N species, respectively, while the NH_3-aged limonene SOA contained 12% and 5% of 1N and 2N species. The increase in nitrogen-containing species is accompanied by a shift in the distribution of oxygen atom containing species toward molecules with a lower number of oxygen atoms. The change in the distribution of the number of N and O atoms for the limonene SOA observed in this study is similar to that of Laskin *et al.* (2010)[21] observed for limonene SOA aged with NH_3 on a filter.

Laskin *et al.* (2010) proposed that condensation reactions associated with a substantial increase in the Double-Bond-Equivalent (DBE) values of neutral molecules are responsible for the formation of light-absorbing products. DBE values were determined from the elemental formulae of the identified peaks as described by Laskin *et al.* (2010)[21] (see their eqn (3)). Fig. 5 compares the DBE *vs.* *m*/*z* for the aged and unreacted α-pinene SOA and limonene SOA. The DBE values of the unreacted and aged α-pinene SOA samples show a small difference between them; whereas the DBE values for the aged limonene SOA show a more significant difference in the 250–550 *m*/*z* range from the unreacted limonene SOA and both α-pinene SOA samples. These highly conjugated species also appeared in the same range of *m*/*z* in the Laskin *et al.* (2010)[21] limonene SOA samples, and are potentially responsible for the orange color observed in the aged limonene SOA filter.

ToF-AMS analysis. Using a ToF-AMS, we measured the mass spectra of α-pinene and limonene SOA, with and without NH_3-aging. Based on the Updyke *et al.* (2012)[23] study and the visual observations of the filter samples, we expect to see evidence of chemical changes

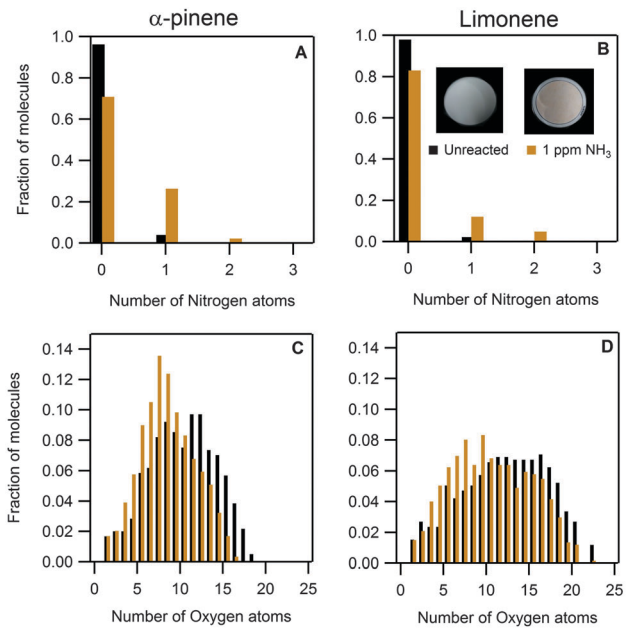

Fig. 4 Distribution of the number of N atoms (top panels) and O atoms (bottom panels) from the identified peaks in the nano-DESI/HR-MS spectra of unreacted (black bars) and NH_3-aged (orange bars) α-pinene SOA (left panels) and limonene SOA (right panels). The picture insets in panel B are the limonene filter samples.

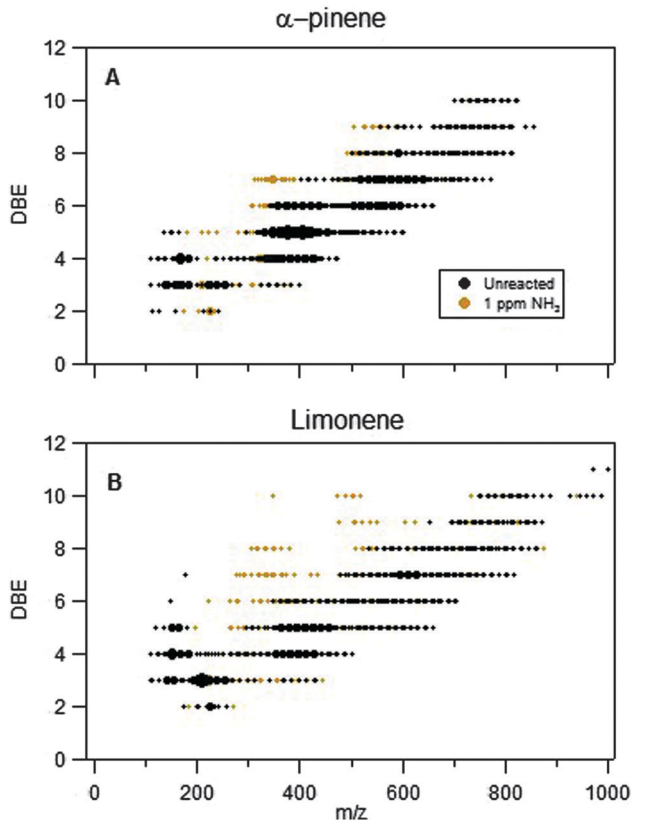

Fig. 5 DBE dependence on the *m*/*z* values for all peaks in the nano-DESI-HRMS spectra. Comparison of the unreacted (black) and aged (orange) α-pinene SOA (top) and limonene SOA (bottom). The size of the points is proportional to the normalized peak intensity.

in the NH_3-aged limonene SOA and have focused our analysis on that aerosol. Due to ion fragmentation inherent to the AMS, it is very difficult if at all possible to unambiguously assign molecular formulas to peaks with $m/z > 100$. The assigned formulae in this analysis are the best estimates based on the information from the nano-DESI/HR-MS data.

It has been shown that ketoaldehydes limononaldehyde (LA) and ketolimononaldehyde (KLA) are abundant and reactive products obtained from the ozonolysis of limonene.[85] The first-generation products are semi-volatile (exist mainly in the gas phase), while the second-generation products are less volatile and are predominantly found in the aerosol phase. Nguyen *et al.* (2013)[84] reported that the unique molecular structure of KLA produces visible-light-absorbing compounds when exposed to ammonia. The KLA–NH_3 reactions produce water-soluble, hydrolysis-resilient chromophores with high mass absorption coefficients, while the first generation ozonolysis product in the oxidation of limonene, limononaldehyde (LA,$C_{10}H_{16}O_2$), does not produce light-absorbing compounds following the reaction with ammonia. For this reason we only focus on the KLA products. Fig. 6 shows a mass spectrum normalized to the total organics in the m/z range between 168 to 360 for the unreacted limonene SOA and the aged limonene SOA. The second-generation ozonolysis product of limonene ($C_{10}H_{16}$), ketolimononaldehyde (KLA, $C_9H_{14}O_3$, $m/z = 170$), can be seen only in the unreacted limonene SOA. The chemistry that produces brown carbon is diverse, with structures of the chromophoric compounds that may be similarly varied in nature, and as mentioned by Nguyen *et al.* (2013),[84] it would not be possible to predict the occurrence of these reactions from average properties of aerosols alone, such as the O/C ratio, which is frequently used in correlating physical properties to the average composition. However, Nguyen *et al.* (2013)[84] also reported that the KLA browning reaction generates a diverse mixture of light-absorbing compounds, with the majority of the observable products containing 1–4 units of KLA and 0–2 nitrogen atoms. An example of such a product found after the reaction containing two nitrogen atoms ($C_9H_{14}O_3N_2$) is shown in Fig. 6. The unique reaction products with high DBE detected after the reaction are also shown in Fig. 6. Examples of such products include $C_{20}H_{24}O_2N_2$ and $C_{21}H_{26}O_3N_2$ which have a DBE of 10, and $C_{20}H_{26}O_4N_2$ which has a DBE of 9. These examples show that high DBE values appeared in both the ToF-AMS and nano-DESI/HR-MS measurements only after the reaction with ammonia.

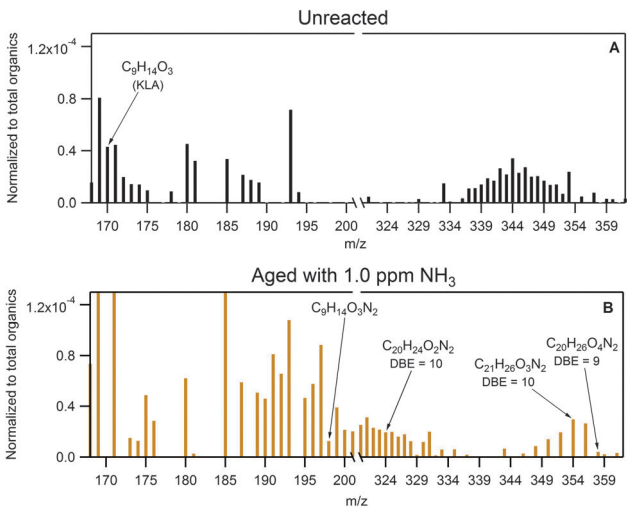

Fig. 6 Mass spectra normalized to the total organics for the unreacted (black, top panel) and the NH_3-aged limonene SOA (orange, bottom panel) measured by the ToF-AMS. Ketolimononaldehyde (KLA; a main product of limonene ozonolysis) is identified. Reaction products with high DBE that were observed in the nano-DESI/HR-MS filter analysis are also identified.

3.5. Comparison of alkene + O_3 SOA without NH_3-aging to literature refractive index values

Recently, there have been an increasing number of studies that retrieved complex refractive indices of SOA generated from monoterpenes.[53,55–61,64,86,87] They are summarized in Table 1. Among these studies, only a few gave values in the near-UV spectral region (marked in bold in Table 1). For example, for SOA generated from the ozonolysis of α-pinene, Schnaiter *et al.* (2003)[53] reported a constant value of $n = 1.44$ for $\lambda > 350$ nm determined by measuring the wavelength dependence of the SOA scattering and extinction. Using cavity ring down spectroscopy (CRDS), Nakayama *et al.* (2010)[57] reported a value of $n = 1.458$ (± 0.019) at $\lambda = 355$ nm, and Nakayama *et al.* (2012)[59] found values between $n = 1.475$ (± 0.022) and $n = 1.463$ (± 0.019) at $\lambda = 405$ nm. Recently, Liu *et al.* (2013)[64] using variable angle spectroscopic ellipsometry reported real part values of $n = 1.517$ (± 0.003) and $n = 1.509$ (± 0.003) for $\lambda = 360$ nm and $\lambda = 420$ nm, respectively. The imaginary components they found in this range were below $k < 10^{-4}$. Using a potential aerosol mass (PAM) flow tube reactor to form SOA by homogeneous nucleation and condensation following OH oxidation of α-pinene at different oxidation levels, Lambe *et al.* (2013)[87] found RI values between $n = 1.51$ (± 0.02) and $n = 1.45$ (± 0.04) with imaginary part values of $k < 0.001$ at $\lambda = 405$ nm, using a CRDS and a photo-acoustic sensor. The values retrieved in our study using BBCES vary from $n = 1.48$ (± 0.03) at $\lambda = 420$ nm to $n = 1.52$ (± 0.02) at $\lambda = 360$ nm. These values are consistent with the values reported previously and show a small spectral dependence with increasing value of the real part of the refractive index with decreasing wavelength.

For SOA generated from the ozonolysis of limonene, we could only find one recent study that gives the RI in the near UV spectral region. Liu *et al.* (2013)[64] measured real parts between 1.520 (± 0.003) at $\lambda = 360$ nm and 1.512 (± 0.003) at $\lambda = 420$ nm and imaginary parts below $<10^{-4}$. Recently, Flores *et al.* (2014)[63] measured the RI of SOA formed by the ozonolysis of a 1 : 1 mixture of α-pinene and limonene in the SAPHIR chamber in Jülich, Germany, using BBCES. They found values varying from $n = 1.511$ (± 0.011) at $\lambda = 360$ nm to 1.485 (± 0.010) at $\lambda = 420$ nm and no detectable absorption. In the visible range of the spectrum, Kim and Paulson (2013)[86] measured the RI at $\lambda = 532$ nm for the ozonolysis of limonene and found values for the real part of the RI varying from $n = 1.4$ to 1.5.

For α-humulene we could not find any studies that give the RI in the near UV spectral region to compare with our measurements.

Table 1 Complex refractive index values of SOA from monoterpenes

Complex refractive index					
Real part (n)	Imaginary part (k)	VOC	SOA formation	Wavelength (nm)	Ref.
1.44	**NA**	**α-Pinene**		**>350**	**Schneiter *et al.* (2003)[53]**
1.45	NA	α-Pinene		Visible	Wex *et al.* (2009)[55]
1.4–1.5	NA	α-Pinene and β-pinene		670	Kim *et al.* (2010)[56]
1.458 (±0.019)	$\mathbf{0.000}(^{+0.021}_{-0.000})$	**α-Pinene**		**355**	**Nakayama *et al.* (2010)[57]**
1.411 (±0.021)	$0.000(^{+0.025}_{-0.000})$	α-Pinene		532	Nakayama *et al.* (2010)[57]
1.49–1.51	0	α-Pinene		532	Redmond and Thompson (2011)[62]
1.475 (±0.022)–1.463 (±0.019)	$\mathbf{0.000}(^{+0.001}_{-0.000})-\mathbf{0.000}(^{+0.001}_{-0.000})$	**α-Pinene**		**405**	**Nakayama *et al.* (2012)[59]**
1.476 (±0.021)–1.466 (±0.02)	$0.000(^{+0.001}_{-0.000})-\mathbf{0.000}(^{+0.002}_{-0.000})$	α-Pinene	Ozonolysis	532	Nakayama *et al.* (2012)[59]
1.410 (±0.028)–1.400 (±0.032)	$0.001(^{+0.002}_{-0.001})-0.001(\pm0.001)$	α-Pinene		781	Nakayama *et al.* (2012)[59]
1.579–1.491 (1.516–1.509)	**<0.01 (<10^{-4})**	**α-Pinene**		**200–1200 (360–420)**	**Liu *et al.* (2013)[64]**
1.590–1.492 (1.520–1.512)	**<0.01 (<10^{-4})**	**Limonene**		**200–1200 (360–420)**	**Liu *et al.* (2013)[64]**
1.52 (±0.02)–1.48 (±0.03)	$\mathbf{0.000}(^{+0.002}_{-0.001})-\mathbf{0.000}(^{+0.021}_{-0.000})$	**α-Pinene**		**360–420**	**This study**
1.57 (±0.02)–1.52 (±0.03)	$\mathbf{0.000}(^{+0.024}_{-0.000})-\mathbf{0.000}(^{+0.050}_{-0.000})$	**Limonene**		**360–420**	**This study**
1.48 (±0.02)–1.45 (±0.03)	$\mathbf{0.000}(^{+0.011}_{-0.000})-\mathbf{0.000}(^{+0.021}_{-0.000})$	**α-Humulene**		**360–420**	**This study**
1.42 (±0.02)	NA	α-Pinene		670	Barkey *et al.* (2007)[94]
1.56 (±0.04)	NA	α-Pinene	Photo-oxidation in	450	Yu *et al.* (2008)[54]
1.51 (±0.03)	NA	α-Pinene	the presence of NO_x	550	Yu *et al.* (2008)[54]
1.46 (±0.03)	NA	α-Pinene		700	Yu *et al.* (2008)[54]
1.4–1.53	NA	α-Pinene		670	Kim *et al.* (2010)[56]
1.38–1.53	NA	β-Pinene		670	Kim *et al.* (2010)[56]
1.53 (±0.08)	$0.00(^{+0.05}_{-0.00})$	Emitted from Holm Oak	Photo-oxidation	532	Lang-Yona *et al.* (2010)[61]
1.498 (±0.022)	$\mathbf{0.000}(^{+0.001}_{-0.000})$	**α-Pinene**		**405**	**Nakayama *et al.* (2012)[59]**
1.458 (±0.021)	$0.000(^{+0.001}_{-0.000})$	α-Pinene		532	Nakayama *et al.* (2012)[59]
1.422 (±0.028)	$0.000(^{+0.002}_{-0.000})$	α-Pinene		781	Nakayama *et al.* (2012)[59]
1.51 (±0.02)–1.45 (±0.04)	**<0.001**	**α-Pinene**	OH oxidation	**405**	**Lambe *et al.* (2013)[87]**
1.511 (±0.011)–1.485 (±0.010)	**0**	**Mixture of α-pinene and limonene**	**Ozonolysis and OH oxidation**	**360–420**	**Flores *et al.* (2014)[63]**

The near-UV measurements are marked in bold.

3.6. Atmospheric implications for the measured refractive indices of NH_3-aged biogenic SOA

The organic aerosol aging experiments described here use biogenic VOC concentrations of 10 ppmv and NH_3 concentrations between 0.3 and 1.9 ppmv. Although these mixing ratios are high, relative to ambient values, it has been shown that the chemical composition of limonene SOA formed at high reagent concentrations in a flow tube is similar to that formed with <0.1 ppm mixing ratios in a smog chamber.[88] Furthermore, Kourtchev *et al.* (2014)[89] reported that SOA formed in an atmospheric simulation chamber by the ozonolysis of α-pinene, represents reasonably well the overall composition of ambient samples obtained from a boreal forest. Ammonia represents the primary form of reactive nitrogen in the atmosphere, with emissions of 45–85 Tg N yr^{-1} estimated in 2008.[90] Summertime measurements of ambient NH_3 in southern and central California in 2010 ranged from 10 to 100 ppbv, with values up to 250 ppbv downwind from confined animal dairy facilities.[91] Satellite measurements of NH_3 in 2008 identify 26 additional global hotspots with annually-averaged columns greater than 0.5 mg m^{-2} (equivalent to 0.7 ppbv for a 1000 m planetary boundary layer).[92] If we assume that the NH_3 aging reactions may scale linearly with time and concentration (an assumption that needs verification), then 1.5 h reaction with 1 ppm NH_3 would be equivalent to 24 h reaction with 63 ppbv NH_3, indicating that the laboratory measurements explore the full range of atmospherically-relevant NH_3 gas-phase concentrations.

Table 2 summarizes MAC and k values from different field and laboratory studies reported in the literature. The absorption values measured here for NH_3-aged aerosol are similar in magnitude to these values. Besides the Lack *et al.* (2012)[6] study, our values fall at the lower end of the absorption in the near ultraviolet spectral region. These differences might come from the fact that we do not know what parts of the ambient measurements are aged biogenic SOA and which are primary pollution or mineral dust. Here we considered only biogenic SOA generated from the reaction of biogenic alkenes with O_3 and its subsequent browning by NH_3. The low k values ($k < 0.01$ for all NH_3 concentrations less than 1 ppm) are generally

Table 2 Values of MAC and imaginary part values for different field and laboratory studies

MAC (m^2 g^{-1})	Imaginary part (k)	Wavelength (nm)	SOA	Ref.
5–0	0.19–0[a]	350–700	Biomass combustion	Kirchstetter *et al.* (2004)[10]
8–0	0.27–0[a]	300–700	Combustion	Sun *et al.* (2007)[96]
10–0	0.238–0	300–500	Organic carbon (Mexico City)	Barnard *et al.* (2008)[97]
2.8[a]	0.11 (±0.02)	355	Organic soluble from diesel soot	Adler *et al.* (2010)[98]
1.7[a]	0.07 (±0.01)	355	Water-soluble from diesel soot	Adler *et al.* (2010)[98]
0.77	0.031[a]	365	Water-soluble (Atlanta and Los Angeles)	Zhang *et al.* (2011)[13]
0.19	0.008[a]	365	Primary BrC (Atlanta and Los Angeles)	Zhang *et al.* (2011)[13]
0.01–1	0.0006–0.040[a,b]	Near 500	Primary BrC	Updyke *et al.* (2012)[23] and references in their Table 2
0.0002[a]	0.007 (±0.005)	404	Forest fire (Boulder)	Lack *et al.* (2012)[6]
0	0	532	Forest fire (Boulder)	Lack *et al.* (2012)[6]
0–0.02	0–0.001	405	OH oxidation of α-pinene	Lambe *et al.* (2013)[87]
0.02–0.09	0.001–0.0035	405	OH oxidation naphtalene[c]	Lambe *et al.* (2013)[87]
<0.25[a]	<0.01[d]	360–420	Ozonolysis of α-pinene, limonene and α-humulene	This study

[a] Calculated assuming a $\rho_{material}$ = 1.4 g cm^{-3}. [b] Calculated at λ = 500 nm. [c] Measured substance with the greatest increase in MAC from naphthalene, guaiacol, tricycle[5.2.$10^{2,6}$]-decane, and α-pinene. [d] For [NH_3] < 1 ppm.

consistent with the small MAC and k values observed for brown carbon in the atmosphere.

To test the impact from the greatest change in the imaginary part of the retrieved RI values on aerosol optical properties and radiative forcing at the Earth's surface, we use the "simple forcing efficiency" proposed by Bond and Bergstrom (2006).[68] The calculation of the SFE is a simple calculation to determine atmospheric importance,[76] while a full radiative transfer model is needed to accurately determine forcing efficiency. For these calculations, we assume an average earth surface albedo of 0.19, a density of ρ = 1.4 g cm^{-3}, and a median aerosol diameter of 150 nm for the Mie calculations. Two SFE calculations were done, for each calculation we assume a constant n value of 1.50, and for the values of k we used k = 0.0 and k = 0.05 (the upper bound from the average change in k observed in the α-humulene and limonene SOA). These assumptions were made to obtain the maximal change in the forcing efficiency, since the k value ought to be wavelength dependent over the 360–910 nm range.

Fig. 7 shows the SFE for the two cases for wavelengths between 360 and 910 nm. The integrated forcing for the m = 1.5 + 0.0i case (black line) is −28 W g^{-1}, and for the m = 1.5 + 0.05i case is −9.6 W g^{-1}. These observed changes in the refractive index due to aging by NH_3 indicate that the cooling effect by the aerosol can decrease by a factor of three. This drastic change may only occur where NH_3 concentrations reach levels >1 ppm, as has been observed in forest fire plumes,[93] or where aerosol is exposed to more moderate levels of NH_3 (~60 ppbv) for 24 h.

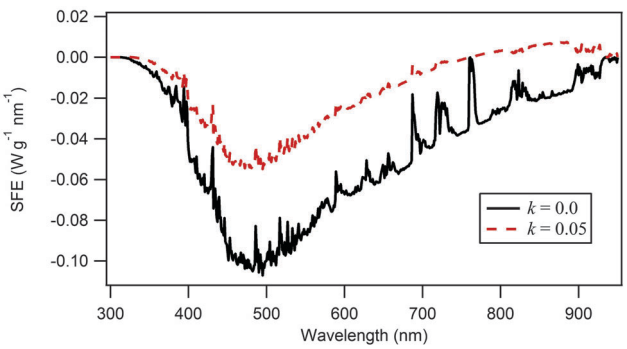

Fig. 7 Simple forcing efficiency calculated assuming a constant real part of n = 1.5 and two different imaginary parts: k = 0.0 (black line) and k = 0.05 (red dashed line).

4. Summary and conclusions

We measured the change in the complex refractive index in the 360–420 nm wavelength range for SOA formed by the ozonolysis of α-pinene, limonene, and α-humulene (three biogenic VOC precursors), when exposed to different concentrations of NH_3. For the α-pinene SOA there was a change in the real part of the RI from an average n = 1.50 (±0.01) for the unreacted SOA to n = 1.57 (±0.01) after a 1.5 h exposure to 1.9 ppm NH_3. For limonene SOA and α-humulene SOA, we observed a small change in the imaginary component of the RI. The imaginary component increased to an average k = 0.029 (±0.021) for α-humulene SOA, and to an average k = 0.032 (±0.019) for limonene SOA after a 1.5 h exposure to 1.3 and 1.9 ppm of NH_3, respectively. Collected filter samples of aged and unreacted α-pinene SOA and limonene SOA were analyzed by nano-DESI/HR-MS, and *in situ* using a ToF-AMS, confirming that the chemical reaction occurred and that N-containing reaction products were formed. The NH_3-aged limonene SOA filter changed to light orange in color, indicating the formation of light-absorbing products. The nano-DESI/HR-MS analysis showed that the number of N-containing molecules increases significantly from the unreacted samples. Furthermore, there are indications that high double bond equivalent values are needed for the formation of brown carbon. The ToF-AMS analysis showed products which appear only after the reaction with NH_3 occurred and were also shown to have high DBE values. If we assume that NH_3 aging reactions scale linearly with time and concentration, then a 1.5 h reaction with 1 ppm NH_3 in the laboratory is equivalent to 24 h reaction with 63 ppbv NH_3, indicating that the observed aerosol absorption will be limited to atmospheric regions with high NH_3 concentrations.

To assess the sensitivity of the BBCES RI retrievals, we measured atomized samples of a humic-like substance proxy, Suwannee River fulvic acid, and a filter extract of NH_3-aged limonene SOA

generated at UC-Irvine, which was light orange in color. We found k values of the order of 0.05 for SRFA and no detectable absorption for the NH_3-aged limonene SOA in the 360–420 nm range. UV/Vis absorption spectra were used to determine mass absorption coefficients and k values for SRFA, NH_3-aged limonene SOA generated at UC Irvine, and NH_3-aged limonene SOA generated in this study. SRFA showed approximately an order of magnitude greater absorption than the two NH_3-aged limonene SOA samples. We calculated the MAC for the filter samples to be <0.2 m^2 g^{-1}, which corresponds to imaginary parts of 0.008–0.009 for wavelengths between 360 and 420 nm and ρ = 1.4 g cm^{-3}. With such small MAC and k values, the BrC formed by the interaction of biogenic SOA with ammonia is expected to make a significant contribution to the absorption in the atmosphere only where ammonia concentrations are greater than 1 ppm for 1.5 h or where NH_3 exposure times are proportionally longer (*e.g.* 63 ppbv for 24 h). In these cases, the simple forcing efficiency calculation showed that the cooling effect by the aerosol can be decreased by up to a factor of three.

The use of SRFA as a proxy for a humic-like substance proved useful to verify that there were no errors with the instrumental method or the refractive index retrieval, but it also showed that its optical properties, specifically its absorption properties, are significantly higher than those of the NH_3-aged SOA and other BrC measured in the field.[6,95] Therefore, the use of SRFA as a BrC standard should be taken with caution as the absorption can be significantly overestimated.

The *in situ* measurements of aerosol extinction and retrieved complex refractive indices from this study demonstrate that bulk phase experiments of brown carbon can sensitively and reliably identify chemical shifts that lead to absorbing components. However, the *in situ* measurements of aerosol optical properties at relevant atmospheric size distributions provide an essential confirmation of the real atmospheric impact of such absorption, and should be included together with bulk phase experiments when possible. The absorption observed in bulk phase experiments suggests that a variety of potential organic chromophores may give rise to BrC components. However, quantitative assessment of their impact on climate requires *in situ* aerosol optical measurements, such as refractive index retrievals, over a broad spectral range.

Acknowledgements

This research was supported by research grants from the USA-Israel Binational Science Foundation (BSF) grant #2012013 and by the German Israel Science Foundation (grant #1136-26.8/2011). We thank Avi Lavi for his help with the ToF-AMS measurements, and John Nowak and Charles Brock for their helpful suggestions. RAW and SSB acknowledge financial support from the U.S. Department of Commerce, National Oceanic and Atmospheric Administration through Climate Program Office's Atmospheric Chemistry, Carbon Cycle and Climate (AC4) Program. The PNNL and UCI groups acknowledge support by the NOAA AC4 program, awards NA13OAR4310066 (PNNL) and NA13OAR4310062 (UCI). The nano-DESI/HR-MS experiments described in this paper were performed at the Environmental Molecular Sciences Laboratory, a national scientific user facility sponsored by U.S. DOE's Office of Biological and Environmental Research and located at the Pacific Northwest National Laboratory (PNNL). PNNL is operated for U.S. DOE by Battelle Memorial Institute under Contract No. DE-AC06-76RL0 1830. JMF is supported by a research grant from the Jinich Postdoctoral Fellowship.

References

1 S. Solomon, D. Qin, M. Manning, M. Marquis, K. Averyt and M. M. B. Tignor, *et al.*, *Climate Change 2007: The Physical Science Basis*, Cambridge University Press, Cambridge, UK, 2007.
2 M. O. Andreae and V. Ramanathan, *Science*, 2013, **340**, 280–281.
3 R. Bahadur, P. S. Praveen, Y. Xu and V. Ramanathan, *Proc. Natl. Acad. Sci. U. S. A.*, 2012, **109**, 17366–17371.
4 T. C. Bond, S. J. Doherty, D. W. Fahey, P. M. Forster, T. Berntsen, B. J. DeAngelo, M. G. Flanner, S. Ghan, B. Kärcher, D. Koch, S. Kinne, Y. Kondo, P. K. Quinn, M. C. Sarofim, M. G. Schultz, M. Schulz, C. Venkataraman, H. Zhang, S. Zhang, N. Bellouin, S. K. Guttikunda, P. K. Hopke, M. Z. Jacobson, J. W. Kaiser, Z. Klimont, U. Lohmann, J. P. Schwarz, D. Shindell, T. Storelvmo, S. G. Warren and C. S. Zender, *J. Geophys. Res.: Atmos.*, 2013, **118**, 5380–5552.
5 C. E. Chung, V. Ramanathan and D. Decremer, *Proc. Natl. Acad. Sci. U. S. A.*, 2012, **109**, 11624–11629.
6 D. A. Lack, J. M. Langridge, R. Bahreini, C. D. Cappa, A. M. Middlebrook and J. P. Schwarz, *Proc. Natl. Acad. Sci. U. S. A.*, 2012, **109**, 14802–14807.
7 P. S. Monks, C. Granier, S. Fuzzi, A. Stohl, M. L. Williams, H. Akimoto, M. Amann, A. Baklanov, U. Baltensperger, I. Bey, N. Blake, R. S. Blake, K. Carslaw, O. R. Cooper, F. Dentener, D. Fowler, E. Fragkou, G. J. Frost, S. Generoso, P. Ginoux, V. Grewe, A. Guenther, H. C. Hansson, S. Henne, J. Hjorth, A. Hofzumahaus, H. Huntrieser, I. S. A. Isaksen, M. E. Jenkin, J. Kaiser, M. Kanakidou, Z. Klimont, M. Kulmala, P. Laj, M. G. Lawrence, J. D. Lee, C. Liousse, M. Maione, G. McFiggans, A. Metzger, A. Mieville, N. Moussiopoulos, J. J. Orlando, C. D. O'Dowd, P. I. Palmer, D. D. Parrish, A. Petzold, U. Platt, U. Pöschl, A. S. H. Prévôt, C. E. Reeves, S. Reimann, Y. Rudich, K. Sellegri, R. Steinbrecher, D. Simpson, H. ten Brink, J. Theloke, G. R. van der Werf, R. Vautard, V. Vestreng, C. Vlachokostas and R. von Glasow, *Atmos. Environ.*, 2009, **43**, 5268–5350.
8 M. O. Andreae and A. Gelencsér, *Atmos. Chem. Phys.*, 2006, **6**, 3131–3148.
9 R. K. Chakrabarty, H. Moosmüller, L. W. A. Chen, K. Lewis, W. P. Arnott, C. Mazzoleni, M. K. Dubey, C. E. Wold, W. M. Hao and S. M. Kreidenweis, *Atmos. Chem. Phys.*, 2010, **10**, 6363–6370.
10 T. W. Kirchstetter, T. Novakov and P. V. Hobbs, *J. Geophys. Res.: Atmos.*, 2004, **109**, D21208.
11 S. J. Doherty, S. G. Warren, T. C. Grenfell, A. D. Clarke and R. E. Brandt, *Atmos. Chem. Phys.*, 2010, **10**, 11647–11680.

12 A. Hecobian, X. Zhang, M. Zheng, N. Frank, E. S. Edgerton and R. J. Weber, *Atmos. Chem. Phys.*, 2010, **10**, 5965–5977.
13 X. L. Zhang, Y. H. Lin, J. D. Surratt, P. Zotter, A. S. H. Prevot and R. J. Weber, *Geophys. Res. Lett.*, 2011, **38**, L21810.
14 T. C. Bond, *Geophys. Res. Lett.*, 2001, **28**, 4075–4078.
15 R. J. Park, M. J. Kim, J. I. Jeong, D. Youn and S. Kim, *Atmos. Environ.*, 2010, **44**, 1414–1421.
16 C. D. Cappa, T. B. Onasch, P. Massoli, D. R. Worsnop, T. S. Bates, E. S. Cross, P. Davidovits, J. Hakala, K. L. Hayden, B. T. Jobson, K. R. Kolesar, D. A. Lack, B. M. Lerner, S.-M. Li, D. Mellon, I. Nuaaman, J. S. Olfert, T. Petäjä, P. K. Quinn, C. Song, R. Subramanian, E. J. Williams and R. A. Zaveri, *Science*, 2012, **337**, 1078–1081.
17 X. Wang, S. J. Doherty and J. Huang, *J. Geophys. Res.: Atmos.*, 2013, **118**, 1471–1492.
18 T. W. Kirchstetter and T. L. Thatcher, *Atmos. Chem. Phys.*, 2012, **12**, 6067–6072.
19 M. O. Andreae and P. J. Crutzen, *Science*, 1997, **276**, 1052–1058.
20 D. L. Bones, D. K. Henricksen, S. A. Mang, M. Gonsior, A. P. Bateman, T. B. Nguyen, W. J. Cooper and S. A. Nizkorodov, *J. Geophys. Res.: Atmos.*, 2010, **115**, D05203.
21 J. Laskin, A. Laskin, P. J. Roach, G. W. Slysz, G. A. Anderson, S. A. Nizkorodov, D. L. Bones and L. Q. Nguyen, *Anal. Chem.*, 2010, **82**, 2048–2058.
22 T. B. Nguyen, P. B. Lee, K. M. Updyke, D. L. Bones, J. Laskin, A. Laskin and S. A. Nizkorodov, *J. Geophys. Res.: Atmos.*, 2012, **117**, D01207.
23 K. M. Updyke, T. B. Nguyen and S. A. Nizkorodov, *Atmos. Environ.*, 2012, **63**, 22–31.
24 B. Noziere, P. Dziedzic and A. Cordova, *J. Phys. Chem. A*, 2009, **113**, 231–237.
25 N. Sareen, A. N. Schwier, E. L. Shapiro, D. Mitroo and V. F. McNeill, *Atmos. Chem. Phys.*, 2010, **10**, 997–1016.
26 E. L. Shapiro, J. Szprengiel, N. Sareen, C. N. Jen, M. R. Giordano and V. F. McNeill, *Atmos. Chem. Phys.*, 2009, **9**, 2289–2300.
27 G. Yu, A. R. Bayer, M. M. Galloway, K. J. Korshavn, C. G. Fry and F. N. Keutsch, *Environ. Sci. Technol.*, 2011, **45**, 6336–6342.
28 M. H. Powelson, B. M. Espelien, L. N. Hawkins, M. M. Galloway and D. O. De Haan, *Environ. Sci. Technol.*, 2013, **48**, 985–993.
29 D. O. De Haan, L. N. Hawkins, J. A. Kononenko, J. J. Turley, A. L. Corrigan, M. A. Tolbert and J. L. Jimenez, *Environ. Sci. Technol.*, 2010, **45**, 984–991.
30 M. Trainic, A. A. Riziq, A. Lavi, J. M. Flores and Y. Rudich, *Atmos. Chem. Phys.*, 2011, **11**, 9697–9707.
31 M. M. Galloway, P. S. Chhabra, A. W. H. Chan, J. D. Surratt, R. C. Flagan, J. H. Seinfeld and F. N. Keutsch, *Atmos. Chem. Phys.*, 2009, **9**, 3331–3345.
32 R. Volkamer, P. J. Ziemann and M. J. Molina, *Atmos. Chem. Phys.*, 2009, **9**, 1907–1928.
33 M. Trainic, A. A. Riziq, A. Lavi and Y. Rudich, *J. Phys. Chem. A*, 2012, **116**, 5948–5957.
34 M. T. Casale, A. R. Richman, M. J. Elrod, R. M. Garland, M. R. Beaver and M. A. Tolbert, *Atmos. Environ.*, 2007, **41**, 6212–6224.
35 W. Esteve and B. Noziere, *J. Phys. Chem. A*, 2005, **109**, 10920–10928.
36 R. M. Garland, M. J. Elrod, K. Kincaid, M. R. Beaver, J. L. Jimenez and M. A. Tolbert, *Atmos. Environ.*, 2006, **40**, 6863–6878.
37 H. E. Krizner, D. O. De Haan and J. Kua, *J. Phys. Chem. A*, 2009, **113**, 6994–7001.
38 B. Noziere and W. Esteve, *Geophys. Res. Lett.*, 2005, **32**, L03812.
39 B. Noziere, D. Voisin, C. A. Longfellow, H. Friedli, B. E. Henry and D. R. Hanson, *J. Phys. Chem. A*, 2006, **110**, 2387–2395.
40 B. Noziere and W. Esteve, *Atmos. Environ.*, 2007, **41**, 1150–1163.
41 J. Zhao, N. P. Levitt and R. Y. Zhang, *Geophys. Res. Lett.*, 2005, **32**, L09802.
42 M. Z. Jacobson, *J. Geophys. Res.: Atmos.*, 1999, **104**, 3527–3542.
43 N. O. A. Kwamena and J. P. D. Abbatt, *Atmos. Environ.*, 2008, **42**, 8309–8314.
44 J. N. Pitts, K. A. Vancauwenberghe, D. Grosjean, J. P. Schmid, D. R. Fitz, W. L. Belser, G. B. Knudson and P. M. Hynds, *Science*, 1978, **202**, 515–519.
45 J. W. Lu, J. M. Flores, A. Lavi, A. Abo-Riziq and Y. Rudich, *Phys. Chem. Chem. Phys.*, 2011, **13**, 6484–6492.
46 J. L. Chang and J. E. Thompson, *Atmos. Environ.*, 2010, **44**, 541–551.
47 A. Gelencser, A. Hoffer, G. Kiss, E. Tombacz, R. Kurdi and L. Bencze, *J. Atmos. Chem.*, 2003, **45**, 25–33.
48 A. Hoffer, G. Kiss, M. Blazso and A. Gelencser, *Geophys. Res. Lett.*, 2004, **31**, L06115.
49 J. D. Smith, V. Sio, L. Yu, Q. Zhang and C. Anastasio, *Environ. Sci. Technol.*, 2013, **48**, 1049–1057.
50 A. Limbeck, M. Kulmala and H. Puxbaum, *Geophys. Res. Lett.*, 2003, **30**, 1996.
51 A. G. Rincon, M. I. Guzman, M. R. Hoffmann and A. J. Colussi, *J. Phys. Chem. A*, 2009, **113**, 10512–10520.
52 A. G. Rincon, M. I. Guzman, M. R. Hoffmann and A. J. Colussi, *J. Phys. Chem. Lett.*, 2010, **1**, 368–373.
53 M. Schnaiter, H. Horvath, O. Möhler, K. H. Naumann, H. Saathoff and O. W. Schöck, *J. Aerosol Sci.*, 2003, **34**, 1421–1444.
54 Y. Yu, M. J. Ezell, A. Zelenyuk, D. Imre, L. Alexander, J. Ortega, B. D'Anna, C. W. Harmon, S. N. Johnson and B. J. Finlayson-Pitts, *Atmos. Environ.*, 2008, **42**, 5044–5060.
55 H. Wex, M. D. Petters, C. M. Carrico, E. Hallbauer, A. Massling, G. R. McMeeking, L. Poulain, Z. Wu, S. M. Kreidenweis and F. Stratmann, *Atmos. Chem. Phys.*, 2009, **9**, 3987–3997.
56 H. Kim, B. Barkey and S. E. Paulson, *J. Geophys. Res.: Atmos.*, 2010, **115**, D24212.
57 T. Nakayama, Y. Matsumi, K. Sato, T. Imamura, A. Yamazaki and A. Uchiyama, *J. Geophys. Res.: Atmos.*, 2010, **115**, D24204.
58 H. Kim, B. Barkey and S. E. Paulson, *J. Phys. Chem. A*, 2012, **116**, 6059–6067.
59 T. Nakayama, K. Sato, Y. Matsumi, T. Imamura, A. Yamazaki and A. Uchiyama, *Sola*, 2012, **8**, 119–123, DOI: 10.2151/sola.2012-030.
60 T. Nakayama, K. Sato, Y. Matsumi, T. Imamura, A. Yamazaki and A. Uchiyama, *Atmos. Chem. Phys.*, 2013, **13**, 531–545.

61 N. Lang-Yona, Y. Rudich, T. F. Mentel, A. Bohne, A. Buchholz, A. Kiendler-Scharr, E. Kleist, C. Spindler, R. Tillmann and J. Wildt, *Atmos. Chem. Phys.*, 2010, **10**, 7253–7265.
62 H. Redmond and J. E. Thompson, *Phys. Chem. Chem. Phys.*, 2011, **13**, 6872–6882.
63 J. M. Flores, D. F. Zhao, L. Segev, P. Schlag, A. Kiendler-Scharr, H. Fuchs, Å. K. Watne, N. Bluvshtein, T. F. Mentel, M. Hallquist and Y. Rudich, *Atmos. Chem. Phys. Discuss.*, 2014, **14**, 4149–4187.
64 P. Liu, Y. Zhang and S. T. Martin, *Environ. Sci. Technol.*, 2013, **47**, 13594–13601.
65 R. A. Washenfelder, J. M. Flores, C. A. Brock, S. S. Brown and Y. Rudich, *Atmos. Meas. Tech.*, 2013, **6**, 861–877.
66 E. M. Wilson, J. Chen, R. M. Varma, J. C. Wenger and D. S. Venables, in *Radiation Processes in the Atmosphere and Ocean*, ed. R. F. Cahalan and J. Fischer, 2013, vol. 1531, pp. 155–158.
67 W. Zhao, M. Dong, W. Chen, X. Gu, C. Hu, X. Gao, W. Huang and W. Zhang, *Anal. Chem.*, 2013, **85**, 2260–2268.
68 T. C. Bond and R. W. Bergstrom, *Aerosol Sci. Technol.*, 2006, **40**, 27–67.
69 S. E. Fiedler, A. Hese and A. A. Ruth, *Chem. Phys. Lett.*, 2003, **371**, 284–294.
70 R. A. Washenfelder, A. O. Langford, H. Fuchs and S. S. Brown, *Atmos. Chem. Phys.*, 2008, **8**, 7779–7793.
71 R. Thalman and R. Volkamer, *Atmos. Meas. Tech.*, 2010, **3**, 1797–1814.
72 R. M. Varma, D. S. Venables, A. A. Ruth, U. Heitmann, E. Schlosser and S. Dixneuf, *Appl. Opt.*, 2009, **48**, B159–B171.
73 R. M. Varma, S. M. Ball, T. Brauers, H. P. Dorn, U. Heitmann, R. L. Jones, U. Platt, D. Pohler, A. A. Ruth, A. J. L. Shillings, J. Thieser, A. Wahner and D. S. Venables, *Atmos. Meas. Tech.*, 2013, **6**, 3115–3130.
74 E. O. Knutson and K. T. Whitby, *J. Aerosol Sci.*, 1975, **6**, 443–451.
75 A. Wiedensohler, *J. Aerosol Sci.*, 1988, **19**, 387–389.
76 Y. Chen and T. C. Bond, *Atmos. Chem. Phys.*, 2010, **10**, 1773–1787.
77 M. Hallquist, J. C. Wenger, U. Baltensperger, Y. Rudich, D. Simpson, M. Claeys, J. Dommen, N. M. Donahue, C. George, A. H. Goldstein, J. F. Hamilton, H. Herrmann, T. Hoffmann, Y. Iinuma, M. Jang, M. E. Jenkin, J. L. Jimenez, A. Kiendler-Scharr, W. Maenhaut, G. McFiggans, T. F. Mentel, A. Monod, A. S. H. Prevot, J. H. Seinfeld, J. D. Surratt, R. Szmigielski and J. Wildt, *Atmos. Chem. Phys.*, 2009, **9**, 5155–5236.
78 P. F. DeCarlo, J. R. Kimmel, A. Trimborn, M. J. Northway, J. T. Jayne, A. C. Aiken, M. Gonin, K. Fuhrer, T. Horvath, K. S. Docherty, D. R. Worsnop and J. L. Jimenez, *Anal. Chem.*, 2006, **78**, 8281–8289.
79 P. J. Roach, J. Laskin and A. Laskin, *Anal. Chem.*, 2010, **82**, 7979–7986.
80 P. J. Roach, J. Laskin and A. Laskin, *Analyst*, 2010, **135**, 2233–2236.
81 P. J. Roach, J. Laskin and A. Laskin, *Anal. Chem.*, 2011, **83**, 4924–4929.
82 P. Chylek and J. Wong, *Geophys. Res. Lett.*, 1995, **22**, 929–931.
83 Y. Liu and P. H. Daum, *J. Aerosol Sci.*, 2008, **39**, 974–986.
84 T. B. Nguyen, A. Laskin, J. Laskin and S. A. Nizkorodov, *Faraday Discuss.*, 2013, **165**, 473–494.
85 S. Leungsakul, M. Jaoui and R. M. Kamens, *Environ. Sci. Technol.*, 2005, **39**, 9583–9594.
86 H. Kim and S. E. Paulson, *Atmos. Chem. Phys.*, 2013, **13**, 7711–7723.
87 A. T. Lambe, C. D. Cappa, P. Massoli, T. B. Onasch, S. D. Forestieri, A. T. Martin, M. J. Cummings, D. R. Croasdale, W. H. Brune, D. R. Worsnop and P. Davidovits, *Environ. Sci. Technol.*, 2013, **47**, 6349–6357.
88 A. P. Bateman, S. A. Nizkorodov, J. Laskin and A. Laskin, *Phys. Chem. Chem. Phys.*, 2011, **13**, 12199–12212.
89 I. Kourtchev, S. J. Fuller, C. Giorio, R. M. Healy, E. Wilson, I. O'Connor, J. C. Wenger, M. McLeod, J. Aalto, T. M. Ruuskanen, W. Maenhaut, R. Jones, D. S. Venables, J. R. Sodeau, M. Kulmala and M. Kalberer, *Atmos. Chem. Phys.*, 2014, **14**, 2155–2167.
90 M. A. Sutton, S. Reis, S. N. Riddick, U. Dragosits, E. Nemitz, M. R. Theobald, Y. S. Tang, C. F. Braban, M. Vieno, A. J. Dore, R. F. Mitchell, S. Wanless, F. Daunt, D. Fowler, T. D. Blackall, C. Milford, C. R. Flechard, B. Loubet, R. Massad, P. Cellier, E. Personne, P. F. Coheur, L. Clarisse, M. Van Damme, Y. Ngadi, C. Clerbaux, C. A. Skjøth, C. Geels, O. Hertel, R. J. Wichink Kruit, R. W. Pinder, J. O. Bash, J. T. Walker, D. Simpson, L. Horváth, T. H. Misselbrook, A. Bleeker, F. Dentener and W. de Vries, *Philos. Trans. R. Soc., B*, 2013, **368**, 1621.
91 J. B. Nowak, J. A. Neuman, R. Bahreini, A. M. Middlebrook, J. S. Holloway, S. A. McKeen, D. D. Parrish, T. B. Ryerson and M. Trainer, *Geophys. Res. Lett.*, 2012, **39**, L07804.
92 L. Clarisse, C. Clerbaux, F. Dentener, D. Hurtmans and P. F. Coheur, *Nat. Geosci.*, 2009, **2**, 479–483.
93 D. W. T. M. Griffith, W. G. Mankin, M. T. Coffey, D. E. Ward and A. Riebau, In Global Biomass Burning, *Global biomass burining: Atmospheric, climatic, and biospheric implications*, MIT Press, Cambridge, 1991.
94 B. Barkey, S. E. Paulson and A. Chung, *Aerosol Sci. Technol.*, 2007, **41**, 751–760.
95 J. Liu, M. Bergin, H. Guo, L. King, N. Kotra, E. Edgerton and R. J. Weber, *Atmos. Chem. Phys.*, 2013, **13**, 12389–12404.
96 H. L. Sun, L. Biedermann and T. C. Bond, *Geophys. Res. Lett.*, 2007, **34**, L17813.
97 J. C. Barnard, R. Volkamer and E. I. Kassianov, *Atmos. Chem. Phys.*, 2008, **8**, 6665–6679.
98 G. Adler, A. A. Riziq, C. Erlick and Y. Rudich, *Proc. Natl. Acad. Sci. U. S. A.*, 2010, **107**, 6699–6704.